Pergamon

0956-7151(94)E0140-C

Acta metall. mater. Vol. 42, No. 10, pp. 3321–3330, 1994

0956-7151/94 $7.00 + 0.00

BAINITE NUCLEATION FROM MINERAL SURFACES

J. M. GREGG and H. K. D. H. BHADESHIA

Department of Materials Science and Metallurgy, University of Cambridge/JRDC, Pembroke Street, Cambridge CB2 3QZ, England

(Received 24 February 1994)

Abstract—Experiments have been conducted to study the nucleation of bainite at interfaces between ceramic compounds and low-alloy steels. To facilitate this, chemically pure mineral powders were pressure bonded to steel samples. The resulting composite samples were then heat treated to induce transformation, and hence compare the transformation behaviour in the vicinity of the ceramic/steel interface to that within the bulk of the steel. It is found that the minerals may be categorised into three groups, according to their observed efficacy in inducing the nucleation of bainite.The dominant reason for the stimulation of bainite nucleation seems to be a chemical interaction between the mineral and the steel. One noteable exception is TiO, which, within the limits of resolution, appears to remain inert, and yet enhances bainite formation.

INTRODUCTION

Highly organised and aligned microstructures can often be found in steels. Cleavage cracks, or deformation processes find propagation through such microstructures relatively easy. More chaotic microstructures can be expected to offer a greater resistance to crack propagation. This is why many recent steels designed for toughness at low temperatures, have microstructures with large volume fractions of acicular ferrite. Acicular ferrite is bainite, but nucleates intragranularly from the surfaces of non-metallic inclusions within austenite grains [1, 2]. From these point sources, plates of acicular ferrite grow in many directions so that the overall microstructure is chaotic with adjacent plates pointing along different directions. This is in contrast to the less desirable, though common, microstructure in which plates of ferrite, which are nucleated at austenite grain surfaces, tend to align into packets which provide a lower resistance to the propagation of cleavage cracks.

A large number of experiments have been performed to elucidate the chemical nature of non-metallic inclusions which are particularly effective in acicular ferrite production [3–10]. Also, various mechanisms by which the inclusions induce nucleation have been proposed. However, the non-metallic inclusions found in commercial alloys usually consist of many crystalline and amorphous phases [2, 5, 7–9, 11–15], so that identification of the particular phase responsible for producing acicular ferrite nucleation is inherently difficult. These difficulties prompted Strangwood and Bhadeshia [16] to conduct controlled experiments in which pure ceramic phases were pressure bonded to steel in order to create interfaces which could be studied with confidence. Effective ceramics should then cause enhanced transformation in the vicinity of the interface when compared with reaction within the bulk of the steel. Because of the lack of adequate equipment, high hardenability steels were used so that only allotriomorphic ferrite formation could be examined. Here, we report new experiments using a low-alloy steel to study the bainite nucleation induced by various mineral compounds. Bainite and acicular ferrite appear to have the same transformation mechanism [17–20], so that these experiments should aid in the interpretation of acicular ferrite nucleation.

EXPERIMENTAL METHOD

The composition of the low-alloy steel used is shown in Table 1. Unless otherwise stated, Alloy 1 was used. Its relatively high Si content suppresses the formation of carbides which might themselves cause heterogeneous nucleation. The Mn and C concentrations give a sufficiently high hardenability to allow bainite to form without interference from higher temperature reactions such as the allotriomorphic ferrite transformation.

The alloys were received in the form of ~10 mm diameter rods. These were reduced by machining down to 8 mm diameter rods. The bainite-start temperature of the alloy was estimated using a method described elsewhere [21]. A more accurate value was obtained by isothermal transformation experiments at temperatures close to the calculated start temperature, after austenitisation at 1200°C for 10 min. All heat treatments were performed using a Thermecmastor thermomechanical simulator. The equipment is computer-controlled, with computer data collection. The sample is heated by an RF-coil, in an environmental chamber. After spot-welding a Pt–Rh thermocouple to the steel specimen, it is placed between the

Table 1. Chemical composition of the steels used

Alloy	C (wt%)	Si (wt%)	Mn (wt%)	Mo (wt%)	Al (wt%)	O (ppm)	N (ppm)
Alloy 1	0.204	1.95	1.54	0.00	0.01	8	7
Alloy 2	0.30	0.15	<0.02	4.20	0.00	—	—

The term "ppm" refers to the concentration in parts per million by weight.

two ram heads within the specimen chamber. The ram heads are then lowered so that the specimen is held in position, surrounded by the RF induction heating coil. The chamber is then evacuated to a pressure of $\sim 2 \times 10^{-2}$ Pa before commencement of the computer-controlled thermal and mechanical treatment. Microstructural observations showed that bainite was produced during transformation at temperatures up to ~540°C, with Widmanstätten ferrite occurring at higher temperatures. B_s was therefore identified experimentally to be close to ~540°C, which compares with the calculated value of ~560°C [21].

High purity mineral powders were obtained from various chemical synthesis companies. The powdered compound was in each case placed between two 6 mm lengths of the steel rod, as is shown in Fig. 1. In some of the early experiments the centre of the lower cylinder was drilled out to a depth of 2 mm to accommodate the mineral powder. In later experiments this was deemed unnecessary, as it involved extra machining and produced a less intimate steel–mineral interface. Using the Thermecmastor, the steel–mineral assembly was heated to 1200°C for 10 min, during which a compressive load of 400 N (~8 MPa) was applied. This was found to be sufficient to cause the mineral and steel to bond. After the 10 min at high temperature, the load was removed and the specimen was gas quenched (using either helium or nitrogen) at ~40°C s^{-1} to 510°C (i.e. below B_s). It was held for 25s at this temperature before further gas quenching to room temperature.

The bonded specimens were then sectioned in a plane normal to that of the ceramic/steel interface using a Struers Accutom-2 precision high-speed saw. They were hot mounted in conductive bakelite, and prepared for metallography by grinding using SiC paper and polished using 6 μm diamond paste, before etching in 2% Nital. It was found that on some occasions, a part of the oxide that was originally bonded to the steel, was removed during metallographic preparation. This is not a serious problem because most the observations were on the steel, and in any case, many regions could be found where the oxide remained connected to the steel. Scanning electron microscopy and microanalysis were carried out using CAMSCAN S2 and S4; the latter is equipped with an energy dispersive X-ray analysis unit. Transmission electron microscopy was conducted on a PHILIPS 400T (with EDX), 400ST and Jeol 2000FX (with thin-windowed EDX).

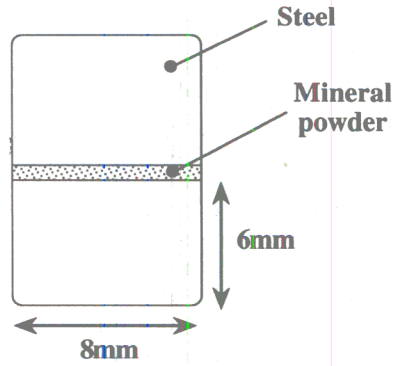

Fig. 1. Schematic diagram of the specimen ready for pressure bonding.

RESULTS

Results from a large number of pressure bonding experiments indicate that minerals fall naturally into three categories, depending on their effects on the steel. These are as follows:

Group I: minerals which appear to react with the steel in a way which induces the nucleation of bainite.

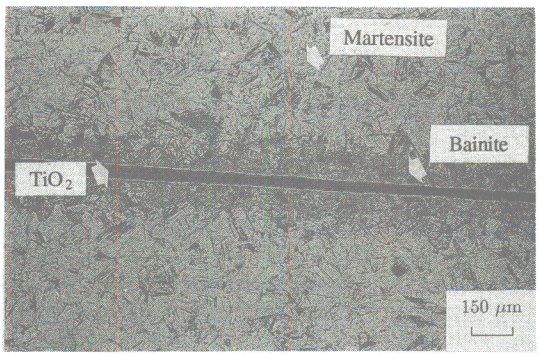

Fig. 2. Profuse bainite nucleation in the interface region between Alloy 1 and TiO_2. Such levels of nucleation are typical of Group I minerals.

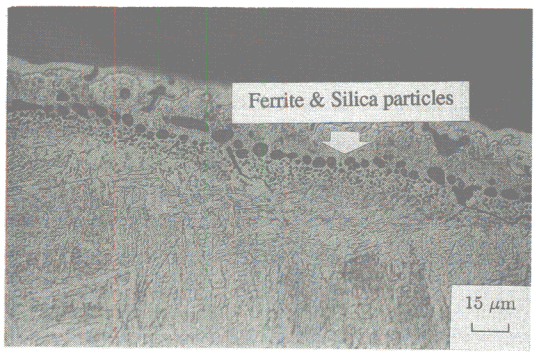

Fig. 3. Optical photomicrograph of the "reaction zone" produced by the Group I minerals.

Table 2. Crystal structure data for TiO_2 and its analogues [25]

Mineral	System	Space group	Lattice parameters/Å
TiO_2	Tetragonal	$P\,4_2/m\,2_1/n\,2/m$	$a = 4.594,\ c = 2.958$
SnO_2	Tetragonal	$P\,4_2/m\,2_1/n\,2/m$	$a = 4.737,\ c = 3.185$
β–MnO_2	Tetragonal (TiO_2 structure)	—	$a = 4.398,\ c = 2.867$
β–PbO_2	Tetragonal	$P\,4/m\,2/m\,2/m$	$a = 4.93,\ c = 3.37$

These include TiO_2, PbO_2, SnO_2, MnO_2, WO_3, MoO_3, V_2O_5 and KNO_3.

Group II: minerals which cause the nucleation of bainite but without any obvious reaction. These include TiO and Ti_2O_3.

Group III: minerals which do not stimulate the production of bainite. These include TiN, $MnAl_2O_4$, γ-Al_2O_3, α-Al_2O_3, NbC, $CaTiO_3$, $SrTiO_3$ and MnS.

Group I

Figure 2 illustrates the profuse nucleation produced adjacent to a Group I mineral which is, in the case illustrated, TiO_2. The steel away from the ceramic has transformed to a much smaller extent than that in the vicinity of the ceramic. Bainite, however, does not emanate directly from the mineral surface. There is, instead, a layer of ferrite in contact with the oxide, which contains spherical particles found to be silicon-rich. This layer extends for $\sim$15–20 μm normal to the ceramic/steel interface (Fig. 3). Beyond this, a thick layer of bainite ($\sim$100 μm) is observable.

A number of experiments were carried out to investigate the reaction layer discussed above. The results indicate that the effects produced by the Group I minerals may be attributed to interactions between the steel and oxygen which originate from the mineral (all group I minerals are capable of liberating oxygen at elevated temperatures). Evidence for the importance of the oxygen–steel interaction is discussed below.

The defect structure of oxides

There has been much interest in the role of titanium oxides in nucleating acicular ferrite in welds [3, 4, 6, 11]. Consequently, titanium oxides were amongst the first minerals to be tested in the bonding experiments. TiO_2 and its structural and behavioural analogues (PbO_2, MnO_2 and SnO_2—Table 2) were all found to exhibit identical features at the steel/ceramic interface. In particular, they all exhibited the reaction zone (Fig. 4).

It has been suggested that the ability of TiO_2 to stimulate ferrite nucleation is linked to the fact that its crystal structure readily permits the formation of oxygen vacancy defects [16, 22]. This is also the case for all the TiO_2-analogues studied here. It seems reasonable to suggest that the liberation of oxygen from such oxides may decarburise the adjacent steel, thereby stimulating the formation of ferrite.

In order to test further the importance of oxygen liberation due to vacancy formation in determining the ability of the mineral to nucleate ferrite, a series of bonding experiments was performed using members of the perovskite mineral group. These minerals were chosen for investigation because it is possible within the same structural group, to find those which have the ability to liberate oxygen, and others which do not. Normal perovskites (ABO_3—Fig. 5) have a similar crystal structure to the defect-perovskites (BO_3—Fig. 6) save for the addition of the large A-atom. The absence of the A-atom in defect-perovskites allows local relaxations in the structure which allow further oxygen loss. Consequently the defect-perovskites are capable of producing many more oxygen vacancies than normal perovskites.

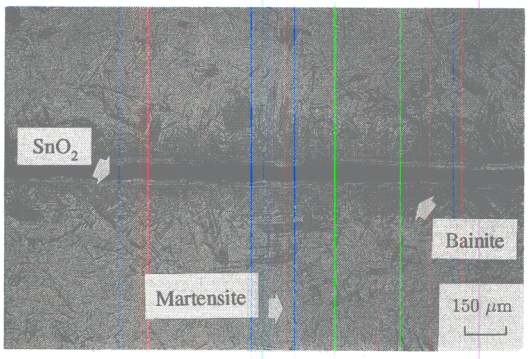

Fig. 4. Analogues of TiO_2 also induce large amounts of transformation—here bainite production is induced by SnO_2.

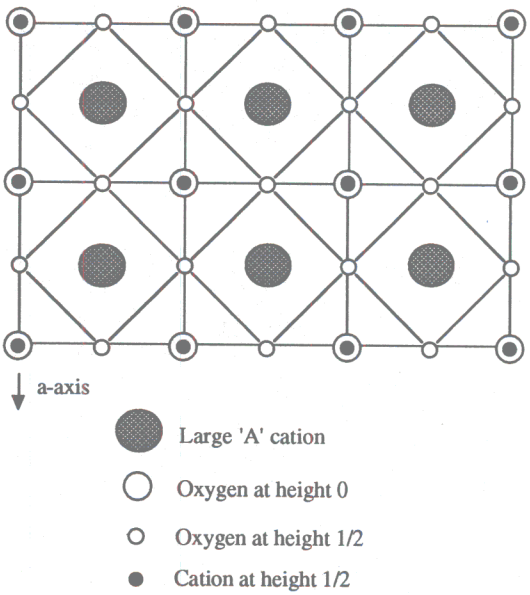

Fig. 5. Structure of the normal perovskites (viewed down [001]).

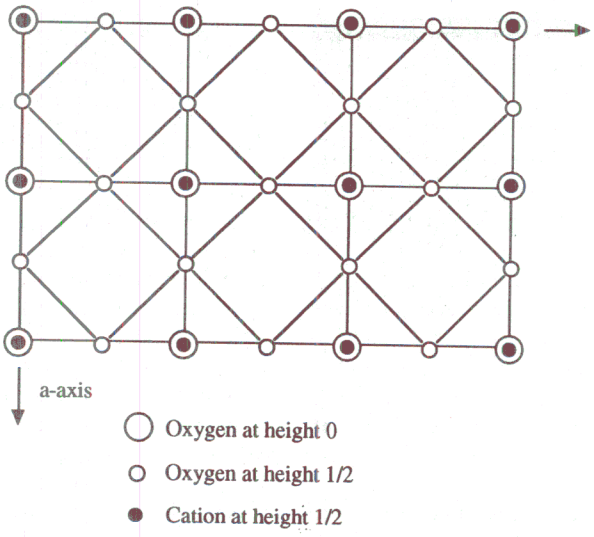

Fig. 6. Structure of the defect perovskite mineral family (viewed down [001])—similar to the normal perovskites save for the absence of the large "A" atom.

Figure 8 shows that defect-perovskites cause classic Group I effects on adjacent steel whereas the normal perovskites (Fig. 7) seem inert, confirming the proposed mechanism for inclusion-stimulated ferrite nucleation. In spite of the structural similarities, only the defect-perovskites were found to be capable of stimulating the formation of bainite.

It follows that any mineral capable of liberating oxygen should stimulate the formation of bainite by the "Group I mechanism". One such mineral is KNO_3 (decomposes at $\sim 400°C$ [23, 24]). As can be seen from Fig. 9, the decomposition of KNO_3 has indeed caused enhanced bainite nucleation at the

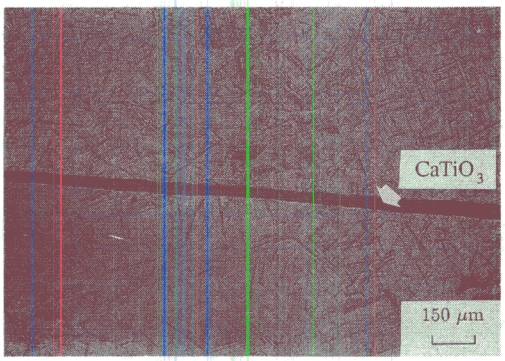

Fig. 7. Normal perovskites do not enhance nucleation of bainite in the local steel.

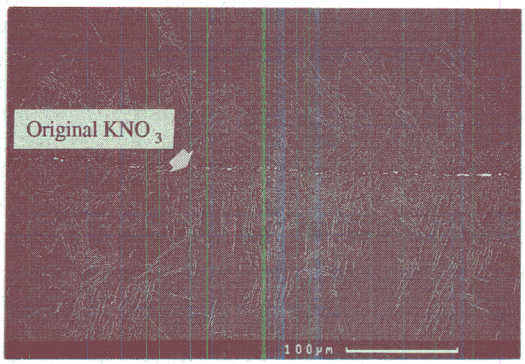

Fig. 9. KNO_3, a mineral which thermally decomposes at 400°C liberating oxygen, also produces local bainite nucleation.

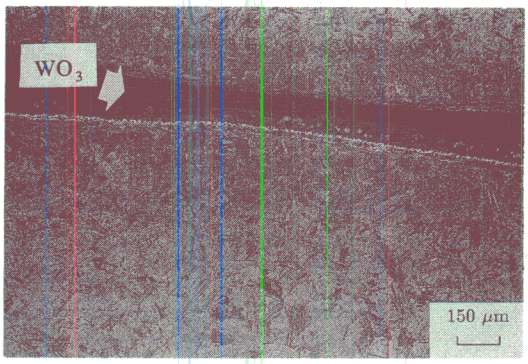

Fig. 8. Defect perovskites cause profuse nucleation of bainite, and obvious reaction zone areas.

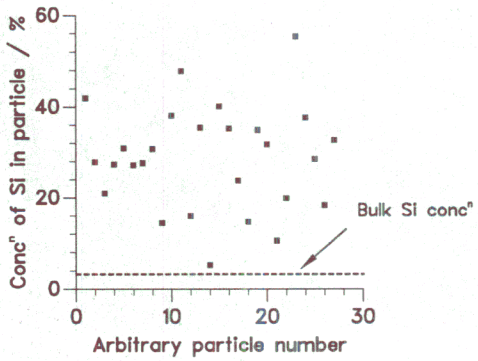

Fig. 10. The particles observable in the KNO_3 bond experiment are Si-rich, as indicated by SEM EDX analysis.

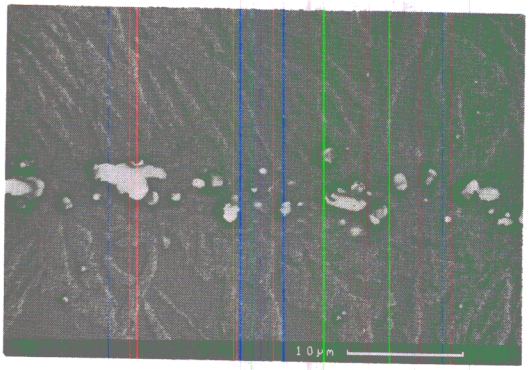

Fig. 11. Si-rich particles produced in the KNO_3 bond experiment are surrounded by ferrite. KNO_3 thus shows all the features associated with the Group I minerals.

KNO_3/steel interface. Furthermore, Si-rich particles are again seen within a ferrite layer at the bond (Figs 10 and 11). Thus decomposition of KNO_3 has induced the occurrence of all the features associated with the Group I minerals. The source of oxygen need not be a mineral—the apparent decarburisation can be induced simply by heat treating in air or in the presence of water vapour (such heat treatments were performed in the thermomechanical simulator either in air, or with water present in the specimen chamber). Figures 12 and 13 show that in both cases bainite formation was stimulated in a manner akin to the TiO_2-effect.

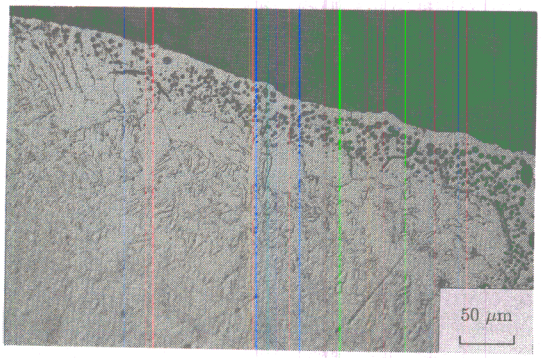

Fig. 12. Exposure of a free surface to air during bonding heat treatment produces a reaction zone.

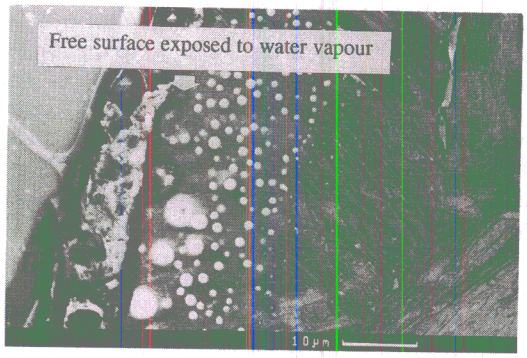

Fig. 13. Exposure of a free surface to water vapour during heat treatment produces a reaction zone.

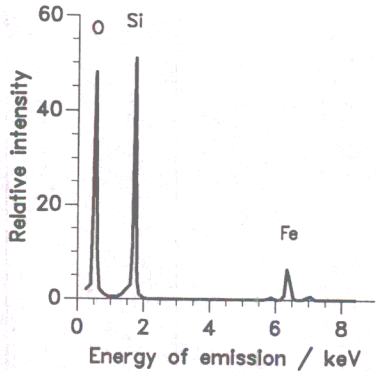

Fig. 14. Thin windowed EDX analysis indicates that the particles in the reaction zone contain oxygen and silicon.

Detailed investigation of the "reaction zone"

Microanalysis of the particles contained within the reaction zone, using a thin-windowed EDX system on TEM thin foils, revealed them to be SiO_x (Fig. 14). The particles were present in a zone extending some 15–20 μm into the steel, away from the TiO_2–steel interface, showing clearly that penetration of oxygen into the steel had occurred.

Changes in the substitutional alloy composition caused by oxygen entry were investigated using SEM EDX. As can be seen from Fig. 15 the reaction zone is depleted in both Mn and Si relative to the bulk chemistry of the alloy, the depletion being limited strictly to the layer of ferrite containing silica particles. The silicon depletion is caused obviously by the precipitation of SiO_x particles, and the manganese depletion by rejection from the growing ferrite allotriomorph which forms the reaction zone, although no Mn peak could be observed outside the ferrite layer.

The possibility that changes in the Mn and Si content in the proximity of the ceramic could have occurred prior to the formation of allotriomorphic ferrite, due to the penetration of oxygen, was investigated further. A pressure bonding experiment was conducted which attempted to prevent the formation of allotriomorphic ferrite, by water-quenching directly from the austenitising temperature. This was

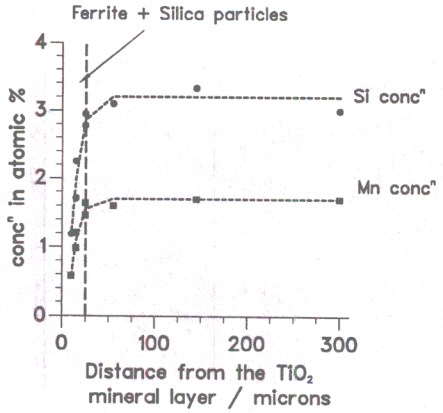

Fig. 15. EDX line profile typical of the steel adjacent to Group I minerals after partial transformation.

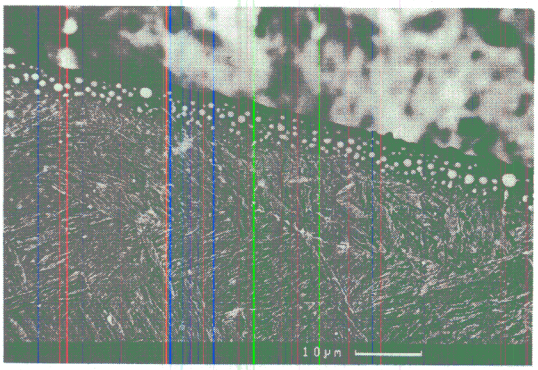

Fig. 16. SEM photomicrograph of the reaction zone adjacent to TiO_2 after water-quenching from 1200°C.

only partly successful in preventing the formation of the reaction zone. The width of the zone produced after water quenching was about 5 μm thick as opposed to the 15–20 μm thickness produced otherwise (Fig. 16). SEM EDX analysis showed that Mn and Si were again depleted near the ceramic, but the depleted region was strictly confined to the reduced extent of the reaction zone (Fig. 17). Most of the diffusion of oxygen into the steel must occur during

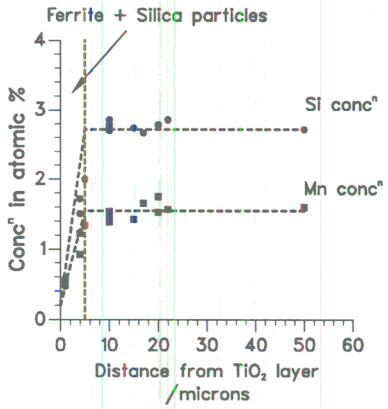

Fig. 17. EDX profile adjacent to TiO_2 after water-quenching from 1200°C. The extent of Mn and Si depletion is confined to the reaction zone which has been reduced to a thickness of about 5 μm.

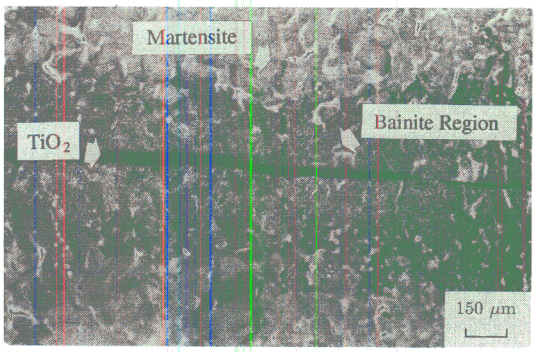

Fig. 18. The nucleation potential of TiO_2 is not apparently dependent on the levels of Si in the steel. Here nucleation is induced in a low Si steel.

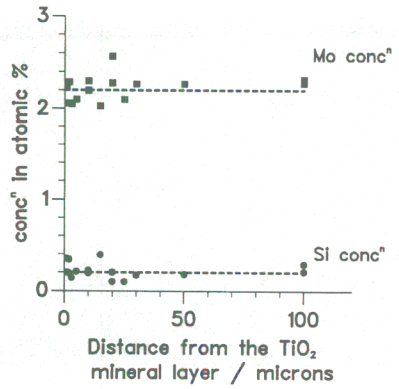

Fig. 19. EDX line profile showing that in the absence of a reaction zone the oxygen produced by TiO_2 has no effect on the substitutional element concentrations in the steel.

the 1200°C heat treatment. Therefore, gas-quenched and water-quenched samples should show similar degrees of oxygen penetration. However, the water-quenched specimen was, as expected, found to contain a thinner layer of ferrite and silica particles than that formed by gas-quenching. The solute depleted zones also became thinner, confirming that the solute changes observed are associated with reaction zone formation rather than oxygen penetration.

Further confirmation was obtained from a series of bonding experiments using Alloy 2 which has a low Si concentration. These experiments were designed to study whether the strong affinity of Si for oxygen is an important factor. As can be seen Fig. 18, despite the low levels of Si in the alloy, significant bainite nucleation was still produced adjacent to the Group I mineral. However, no reaction zone was observed, allowing the observation of oxygen effects on substitutional solutes, without the masking effect of the reaction zone. Fig. 19 shows that the Mo and Si levels remain at the bulk concentration throughout the steel.

The penetration of oxygen into the steel must be accompanied by decarburisation, but the conventional EDX techniques used here were unable to characterise the distribution of carbon. The decarburisation was therefore established indirectly, using a duplex stainless steel which transforms from δ-ferrite to austenite. Any decarburisation in the steel at the ceramic/duplex stainless steel interface should lead to a reduction in the precipitation of austenite in the proximity of the interface, since carbon stabilises austenite. The composition of this steel is given in Table 3. The steel was ferritised at 1350°C for 5 min, gas quenched (40°C s^{-1}) to 1000°C and held for 5 min before gas quenching to room temperature.

Table 3. Composition (wt%) of the duplex stainless steel used

Cr	Ni	Mo	Mn	Si	C
25.9	5.1	3.65	0.67	0.5	0.026

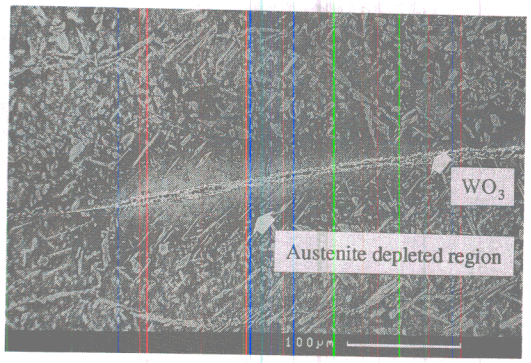

Fig. 20. The inhibition of austenite transformation in this duplex stainless steel in the area adjacent to the Group I mineral (in this case WO_3), demonstrates the possibility of mineral-caused carbon depletion.

Figure 20 shows that the amount of austenite in the region adjacent to the mineral is greatly reduced confirming decarburisation.

To summarise, Group I minerals are those which are capable of liberating oxygen, which in turn causes the decarburisation of the adjacent steel. It is this decarburisation which stimulates the nucleation of bainite. There are some associated effects such as the formation of a reaction zone, which are of secondary importance in the mechanism by which nucleation is stimulated.

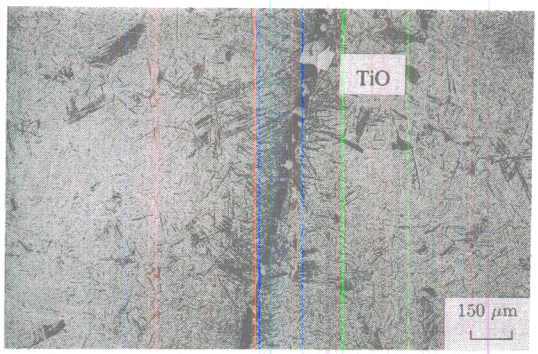

Fig. 21. The TiO/Alloy 1 interface region showing the nucleation produced from the TiO surface.

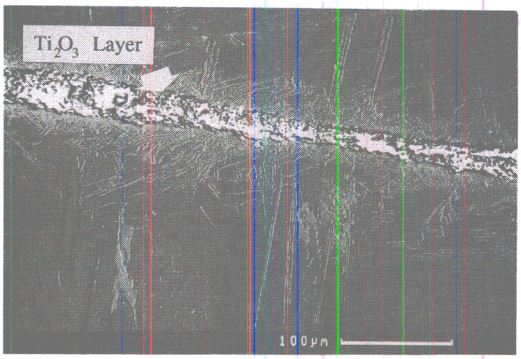

Fig. 22. The Ti_2O_3/steel interface region showing the nucleation produced due to the mineral presence.

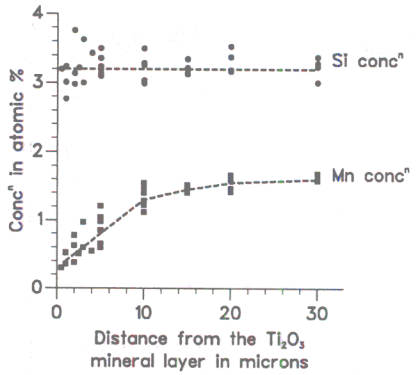

Fig. 23. EDX line profile in steel adjacent to Ti_2O_3. Mn depletion has clearly occurred.

Group II

By contrast with the Group I minerals, two ceramic phases were found not to react with the steel and yet were effective in inducing the nucleation of bainite. These are called the "Group II" minerals. Figures 21 and 22 illustrate the behaviour of TiO and Ti_2O_3. The absence of the reaction zone does not preclude any oxygen–steel interaction, but it indicates that such interaction is unlikely to be the dominant reason for their nucleation potency. SEM EDX analysis of substitutional element concentrations adjacent to Ti_2O_3 revealed a dramatic depletion in the manganese concentration of the adjacent steel (Fig. 23). Since manganese stabilises austenite, such a depletion should stimulate ferrite formation in the vicinity of the Ti_2O_3/steel interface. This manganese depletion is the likely explanation for the effectiveness of the Ti_2O_3 in nucleating bainite. Moreover, microanalysis of the Ti_2O_3 revealed that the manganese diffused into the mineral layer. Ti_2O_3 clearly acts as a manganese sink (Fig. 24).

In order to investigate further, chippings of Alloy 1 were mixed with Ti_2O_3 powder and held at 1200°C for 3 h in an evacuated quartz tube. Subsequent TEM EDX microanalysis of the Ti_2O_3 confirmed significant concentrations of manganese within the oxide

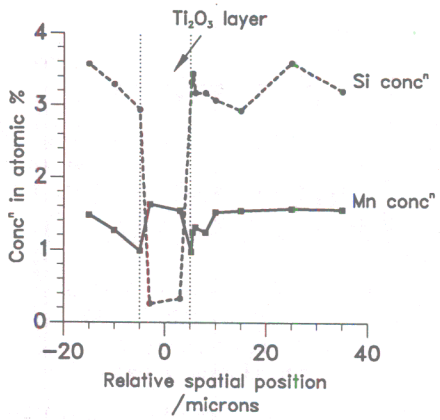

Fig. 24. EDX analysis across a region of Ti_2O_3 shows how the mineral is acting as a Mn sink.

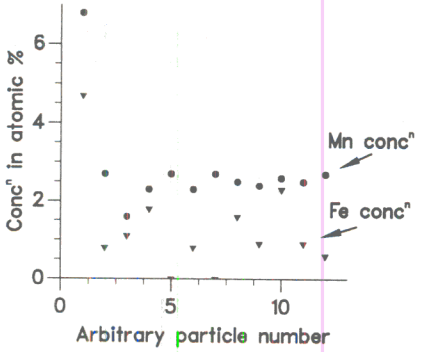

Fig. 25. TEM EDX analysis performed on Ti_2O_3 which had been heated in the presence of Alloy 1 chippings shows that Mn is clearly present in particles. The low levels of Fe recorded show that the Mn detected is not due to EDX information from surrounding steel.

(Fig. 25). X-ray powder diffraction traces and electron diffraction patterns also indicated that the Ti_2O_3 transformed to Ti_3O_5 (Fig. 26).

SEM EDX analysis of the steel adjacent to TiO, however, showed little, if any, difference in substitutional element concentrations between the bulk steel, and steel close to the interface region (Fig. 27).

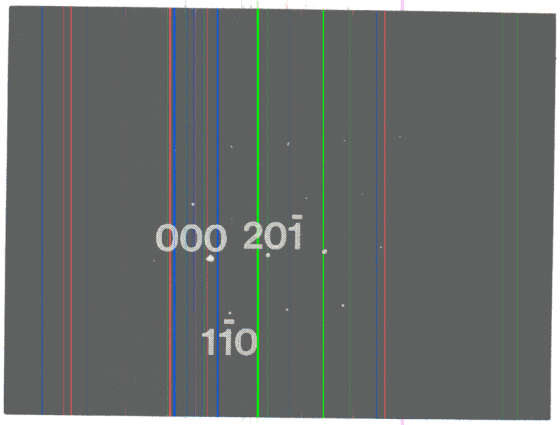

Fig. 26. Diffraction pattern taken from the furnace treated Ti_2O_3 (in the presence of Alloy 1) indexes as Ti_3O_5 and Ti_3O_5.

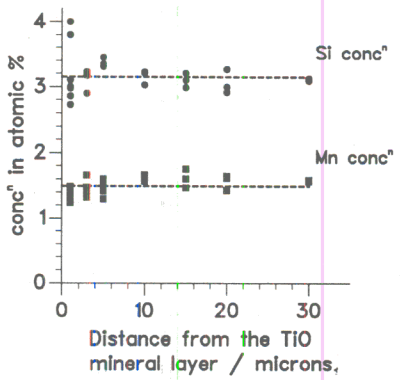

Fig. 27. EDX line profile in steel adjacent to TiO. Within the resolution of this technique, no effect on substitutional element concentrations has occurred.

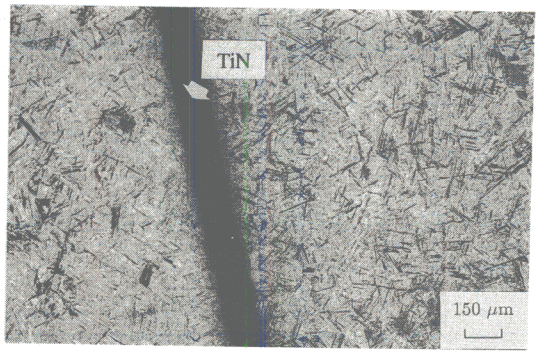

Fig. 28. The interface region between TiN and Alloy 1. There is no extra inducement for bainite production adjacent to the mineral than in the bulk.

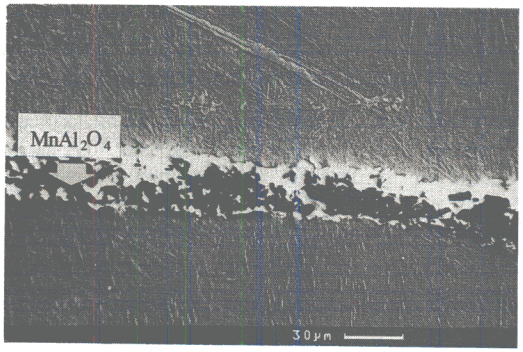

Fig. 29. The interface between galaxite and Alloy 1. No bainite nucleation from the interface can be seen.

Manganese depletion cannot readily account for the potency of TiO in nucleating bainite, at least within the limits of resolution of the microanalytical techniques used.

Group III

This group of minerals was found to remain inert, both chemically and in their ability to stimulate bainite nucleation. Two examples are shown in Figs 28 and 29. There is clearly no extra bainite transformation adjacent to the mineral surfaces over that induced in the bulk of the steel. Minerals which behaved in this manner include α-Al_2O_3 and γ-Al_2O_3, NbC, TiN, $MnAl_2O_4$ and normal perovskites, with MnS found to be only marginally effective. Table 4 summarises the results to date.

Table 4. Summary of the minerals tested and their relative efficacy for stimulating bainite nucleation

Group I (effective)	Group II (effective)	Group III (ineffective)
TiO_2	Ti_2O_3	TiN
PbO_2	TiO	$MnAl_2O_4$
MnO_2		γ-Al_2O_3
SnO_2		α-Al_2O_3
WO_3		NbC
MoO_3		$CaTiO_3$
V_2O_5		$SrTiO_3$
KNO_3		MnS

Table 5. Effectiveness of nucleation viewed against the coefficient of thermal expansion of a selection of the minerals tested

Mineral	Effective nucleant	Coefficient of thermal expansion/K^{-1}	Temp. range of measurement/K	Reference
SnO_2	Yes	4×10^{-6}	273–1073	[25]
		3.76×10^{-6}	295–923	[25]
NbC	No	7×10^{-6}	—	[26]
Al_2O_3	No	8.0×10^{-6}	293–1853	[25]
		8.4×10^{-6}	293–1273	[25]
		7.5×10^{-6}	1273–1573	[25]
		a-axis: 7.1×10^{-6}	373	[25]
		a-axis: 9.7×10^{-6}	773	[25]
		a-axis: 14.2×10^{-6}	1273	[25]
		c-axis: 6.0×10^{-6}	373	[25]
		c-axis: 8.9×10^{-6}	773	[25]
		c-axis: 13.8×10^{-6}	1273	[25]
$MnAl_2O_3$	No	8×10^{-6}	273–1073	[27]
$SrTiO_3$	No	8.9×10^{-6}	273–1080	[28]
TiN	No	9.4×10^{-6}	273–1073	[27]
TiO_2	Yes	9.5×10^{-6}	273–1080	[28]
		7.8×10^{-6}	293–873	[25]
		8.19×10^{-6}	273–773	[25]
$CaTiO_3$	No	1.2×10^{-5}	273–1700	[28]
TiO	Yes	1.4×10^{-5}	273–1400	[28]
MnS	No	1.8×10^{-5}	273–1073	[27]
Austenite	—	2.3×10^{-5}		[27]

DISCUSSION

Although many of the mineral phases utilised in the experiments are unlikely to occur in commercial steels, a number of compounds which do occur have been tested. Specifically TiO, TiN, Ti_2O_3, γ-Al_2O_3, NbC, $MnAl_2O_4$ and MnS. The results show that of these minerals, only TiO and Ti_2O_3 are potent nucleators. Inclusions rich in both TiO and Ti_2O_3 should help maximise yields of acicular ferrite in welds where the alloy design ensures that grain boundary nucleated phases do not overwhelm intragranularly nucleated phases.

The pressure bonding experiments also throw light on the possible mechanisms by which the mineral phases induce nucleation. Minerals in Group I are oxygen sources which cause local decarburisation on the adjacent steel. Ti_2O_3 on the other hand absorbs manganese from the steel, reducing its hardenability, and hence stimulates the nucleation of ferrite.

Lattice matching is a popular explanation for the apparent nucleation potency of the TiX phase (X = C, N or O) in welds [4, 11]. However, the present experiments indicate that TiO acts as a potent nucleant, while TiN does not. Both minerals have a similar lattice match with ferrite [29]. Therefore, the bonding results suggest that a consideration of lattice matching alone cannot distinguish effective from ineffective nucleants.

Differences in the thermal expansion coefficients of inclusion and steel cause strains around an inclusion during cooling. It has been suggested that ferrite transformation adjacent to the inclusion may relieve this strain [12]. Table 5 shows the thermal expansion coefficients of some of the minerals tested. There is clearly no direct correlation between the expansion coefficient difference and bainite nucleation potency, as measured here.

CONCLUSIONS

Chemically pure crystalline minerals, pressure bonded to steels have been used to study the mechanisms by which the minerals stimulate nucleation of ferrite. A number of minerals with defect crystal structures have been found to be capable of liberating oxygen, which then diffuses into the steel. The resulting decarburisation then makes for the easier nucleation of bainite ferrite. Unusually, Ti_2O_3 has been found to act as a manganese sink; the absorbtion of manganese from the steel again reduces hardenability and enhances ferrite formation. The compound TiO, within the limits of resolution, does not react with the steel, but nevertheless stimulates ferrite nucleation for reasons which are not clear. A host of other minerals (notably TiN, galaxite, α-Al_2O_3 and γ-Al_2O_3) are ineffective as bainite nucleants, and it would be appropriate to minimise their presence in welds.

Acknowledgements—The authors are grateful to Professor C. J. Humphreys for the provision of laboratory facilities at the University of Cambridge. JMG would like to thank the Department of Education for Northern Ireland, and ESAB SWEDEN for funding his studies. HKDHB's contribution was via the "Atomic Arrangements: Design and Control Project", which is a collaborative effort between the University of Cambridge and the Research and Development Corporation of Japan.

REFERENCES

1. D. J. Abson, R. E. Dolby and P. Hart, *Welding Institute Research Report*, 67/1978/M (1978).
2. G. S. Barrite, R. A. Ricks and P. R. Howell, *Quantitative Microanalysis with High Spatial Resolution* (edited by G. W. Lorimer), pp. 112–118. The Metals Society, London (1981).
3. H. Terashima, P. H. M. Hart, *Int. Conf. on the Effects of Residual Impurity and Microalloying Elements on Weldability and Weld Properties*, T. W. I., London (1983).

4. N. Bailey, *Welding Institute Research Report*, 221/1983 (1983).
5. J. M. Dowling, J. M. Corbett and H. W. Kerr, *Metall. Trans.* **17A,** 1611 (1986).
6. H. Homma, S. Ohkita, S. Matsuda and K. Yamamoto, Internal Report, Nippon Steel Corp. (1986).
7. M. Es-Souni and P. A. Beaven, *Surf. Interface Analy.* **16,** 504 (1990).
8. M. Es-Souni, P. A. Beaven and G. M. Evans, International Institute of Welding Document, II-A-847-91 (1991).
9. G. Thewlis, International Institute of Welding Document, IXJ 165 90, pp. 1–11 (1990).
10. I. Watanabe and T. Kojima, *J. Japan Weld. Soc.* **49,** (11), 772 (1980); **50,** (7), 702 (1980).
11. N. Mori, H. Homma, S. Okita and M. Wakabayashi, International Institute of Welding Document, IIW Doc IX 1196 81 (1981).
12. G. S. Barrite and D. V. Edmonds, *Advances in the Physical Metallurgy and Application of Steels*, pp. 126–134. The Metals Society, London (1981).
13. F. J. Barbaro, R. H. Edwards and K. E. Easterling, *7th Natl Conf. AXAA—88*, Aust. X-ray Anal. Association (1988).
14. G. Thewlis, *Joining Mater.* **1/2,** 25 125 (1989).
15. A. O. Kluken and Ø. Grong, *Metall. Trans.* **20A,** 1335 (1989).
16. M. Strangwood and H. K. D. H. Bhadeshia, *Phase Transformations 1987* (edited by G. W. Lorimer), pp. 466–470. Institute of metals, London (1988).
17. A. A. B. Sugden and H. K. D. H. Bhadeshia, *Metall. Trans.* **20A,** 1811 (1989).
18. J. R. Yang and H. K. D. H. Bhadeshia, *Advances in Welding Technology and Science* (edited by S. A. David), pp. 187–191. ASM, Metals Park, Ohio (1987).
19. M. Strangwood and H. K. D. H. Bhadeshia, *Advances in Welding Technology and Science* (edited by S. A. David), pp. 209–213. ASM, Metals Park, Ohio (1987).
20. A. O. Kluken, Ø. Grong and J. Hjelen, *Metall. Trans.* **22A,** 657 (1991).
21. H. K. D. H. Bhadeshia, *Metals Sci.* **16,** 159 (1982).
22. M. Strangwood, Ph.D. thesis, Univ. of Cambridge (1986).
23. N. V. Sidgwick (editor), *Chemical Elements and Their Compounds*, Vol. 1, p. 700. Oxford Univ. Press, London (1950).
24. N. Irving Sax, *Dangerous Properties of Industrial Materials*, pp. 1047. Van Nostrand Reinhold Company, New York (1968).
25. G. V. Samsonov (editor), *The Oxide Handbook*. IFI/Plenum Data Corporation, New York (1973).
26. I. G. Barantseva and V. N. Paderno, *Refractory Carbides* (edited by G. V. Samsonov), pp. 283–285 (1974).
27. D. Brooksbank and K. W. Andrews, *J. I. S. I.* **210.1,** 246 (1972).
28. A. Goldsmith, T. E. Waterman and H. J. Hirschhorn, *Handbook of Thermophysical Properties of Solid Materials*. The Macmillan Co., New York (1961).
29. B. L. Bramfitt, *Metall. Trans.* **1,** 1987 (1970).